Characteristics and error estimations of stratospheric ozone and ozone-related species over Poker Flat (65° N, 147° W), Alaska observed by a ground-based FTIR spectrometer from 2001 to 2003

A. Kagawa, Y. Kasai, N. B. Jones, M. Yamamori, K. Seki, F. Murcray, Y. Murayama, K. Mizutani, T. Itabe

Atmos. Chem. Phys. Discuss., 6, 10299–10339, 2006
www.atmos-chem-phys-discuss.net/6/10299/2006/

Atmospheric Chemistry and Physics Discussions

Characteristics and error estimations of stratospheric ozone and ozone-related species over Poker Flat (65° N, 147° W), Alaska observed by a ground-based FTIR spectrometer from 2001 to 2003

A. Kagawa[1,2], Y. Kasai[2], N. B. Jones[3], M. Yamamori[2,4], K. Seki[2,5], F. Murcray[6], Y. Murayama[2,7], K. Mizutani[2], and T. Itabe[2]

[1]Fujitsu FIP Corporation, Tokyo, Japan
[2]National Institute of Information and Communications Technology, Tokyo, Japan
[3]Wollongong University, Wollongong, Australia
[4]Tsuru University, Yamanashi, Japan
[5]Mitsubishi Electric Corporation, Kanagawa, Japan
[6]University of Denver, Denver, USA
[7]National Institute of Polar Research, Tokyo, Japan

Received: 4 August 2006 – Accepted: 9 October 2006 – Published: 17 October 2006

Correspondence to: A. Kagawa (kagawa.akiko@nict.go.jp)

Abstract

It is important to obtain the year-to-year trend of stratospheric minor species in the context of global changes. An important example is the trend in global ozone depletion. The purpose of this paper is to report the accuracy and precision of measurements of stratospheric chemical species that are made at our Poker Flat site in Alaska (65° N, 147° W). Since 1999, minor atmospheric molecules have been observed using a Fourier-Transform solar-absorption infrared Spectrometer (FTS) at Poker Flat. Vertical profiles of the abundances of ozone, HNO_3, HCl, and HF for the period from 2001 to 2003 were retrieved from the FTS spectra by using Rodgers' formulation of the Optimal Estimation Method (OEM). The accuracy and precision of the retrievals were estimated by formal error analysis. Errors for the total column were estimated to be 5.3%, 3.4%, 5.9%, and 5.3% for ozone, HNO_3, HCl, and HF, respectively. The ozone vertical profiles were in good agreement with profiles derived from collocated ozonesonde measurements that were smoothed with averaging kernel functions that had been obtained with the retrieval procedure used in the analysis of spectra from the ground-based FTS (gb-FTS). The O_3, HCl, and HF columns that were retrieved from the FTS measurements were consistent with Earth Probe/Total Ozone Mapping Spectrometer (TOMS) and HALogen Occultation Experiment (HALOE) data over Alaska within the error limits of all the respective datasets. This is the first report from the Poker Flat FTS observation site on a number of stratospheric gas profiles including a comprehensive error analysis.

1 Introduction

Stratospheric ozone depletion has been observed at mid-latitudes for the past several decades (WMO, 2003). Heterogeneous chemical reactions play an important role in middle latitude ozone loss. Organic halogen species such as CFC's eventually breakdown into inactive forms in the stratosphere, forming reservoir species (e.g., HCl).

ACPD

6, 10299–10339, 2006

Heterogeneous reactions at mid-latitudes result in changes to the partitioning of NO_y and prevent conversion of active halogen species that destroy ozone into inactive ones.

Because the long-term trend in stratospheric ozone is expected to be linked to loading of chlorine and bromine species in the stratosphere, a recent focus of research has been on recovery of the ozone layer, since chlorine loading appears to be near its peak in the stratosphere (Newchurch et al., 2003). However, because ozone variability is not only affected by halogen species but also by other factors such as stratospheric temperature changes coming from increases in greenhouse gases, a cautious approach must be taken in detecting the recovery of the ozone layer as a response to halogen loading in the stratosphere. The detection of this recovery phase has therefore been intensively investigated (Newchurch et al., 2003; Reinsel et al., 2005). Monitoring stratospheric ozone and ozone-related species is still important because of the complicated conditions surrounding the stratospheric ozone layer.

There have been many studies on the variability of stratospheric ozone and ozone-related species from satellite, balloon-borne, and ground-based (gb) observations (e.g., Manney et al., 1997). Because ozone and many ozone-related species have absorptions in the infrared region, Fourier-transform infrared (FTIR) spectrometers are highly suited to measurements of atmospheric molecules related to ozone; they can be used to analyze solar and lunar absorption spectra as well as emissions from the atmosphere. Many molecules have been monitored using ground-based FTS systems within the framework for the network detection of atmospheric composition change (NDACC, http://www.ndsc.ncep.noaa.gov/, formerly NDSC). In particular, minor species related to stratospheric ozone have been extensively studied using ground-based FTS (Goldman et al., 1999; Hase et al., 2004; Nakajima et al., 1997; Paton-Walsh et al., 1997; Pougatchev et al., 1996; Rinsland et al., 2000; Wood et al., 2002). The merit of using ground-based FTS for atmospheric measurements is that an FTS can simultaneously observe many molecules over a wide range of wavelengths. Modern FTS systems are also optically stable and are therefore suited to long-term observations (~10 years).

We have been observing solar absorption spectra over Poker Flat (65.1° N,

147.5° W), Alaska since 1999 by using a high-resolution FTS, as a part of the Alaska Project. The Alaska Project is an international collaboration between the National Institute of Information and Communications Technology (NICT) (formerly the Communications Research Laboratory (CRL)) and the University of Alaska Fairbanks (UAF) in which many instruments are used to investigate the atmospheric environment from the troposphere to the thermosphere (Murayama et al., 2003).

Poker Flat is located between the Arctic region and mid-latitudes. Because it is outside the polar vortex for most of the winter and spring, the gas phase and heterogeneous chemistry over Poker Flat is not affected by polar ozone loss, except for transport of diluted ozone from the polar vortex. Because there have been relatively few observations over the Alaska region compared with other areas in the northern hemisphere, the characterization of ozone variability at this location is scientifically interesting. Ozone retrievals from Poker Flat FTS spectra were reported by Seki et al. (2002). Vertical abundances of O_3 and HNO_3 that were observed using Poker Flat FTS in the spring of 2002 have been validated with Improved Limb Atmospheric Spectrometer (ILAS) II data (Yamamori et al., 2006). The present study is the first report on retrieval, formal error analysis, and the characteristics of the seasonal cycles of O_3, HNO_3, HCl, and HF from the Poker Flat site.

To investigate the seasonal change in stratospheric ozone and ozone-related species over Poker Flat, vertical profiles of ozone, HNO_3, HCl, and HF for the years 2001–2003 were retrieved during a period of intensive measurement. These molecules were selected because they have important effects on ozone. HNO_3 and HCl are major reservoir species of NO_y and chlorine. HF is extremely stable and usually referred to as a dynamic tracer. In order to discuss the seasonal and inter-annual variability of stratospheric species, it is important to have (a) continuous observations, (b) simultaneous observations of many species, and (c) measurements with high precision and accuracy. For the purpose of (c), random and systematic errors of the retrieved species were calculated using formal error analysis procedures (Rodgers, 2000), and these species were compared with balloon-borne and satellite data. The FTS observations

ACPD
6, 10299–10339, 2006

EGU

at Poker Flat are described in Sect. 2. The retrieval algorithm and analysis are discussed in Sect. 3. Section 4 presents the retrieval results, and Sect. 5 discusses the retrieval errors. In Sect. 6, the retrieved chemical species are compared with other observations. Section 7 describes the seasonal cycles of the retrieved species. A summary of all of the results is given in Sect. 8.

2 Observation

This section describes the observation technique and basis of the retrieval analysis of the FTS measurements. The FTS instrument, a Bruker 120 HR, was installed at Poker Flat in July 1999.

Its observation frequency range and frequency resolution at a maximum OPD of 360 cm are 750.0–4200.0 cm^{-1} (2.5 μm–13.5 μm) and 0.0019 cm^{-1}, respectively. It uses a KCl beam splitter, and it has seven consecutive optical filters to reduce the broadband signal (avoiding detector non-linearity). Two detectors, a mercury-cadmium-telluride (MCT) one and indium antimonide (InSb) one, were used for the spectral region. The filters, the wavenumber ranges, and the detecter used for the measurements are shown in Table 1.

In order to keep the scan times for a single measurement to less than 10 min (to limit the change in airmass), the frequency resolution for the solar absorption spectrum was reduced to 0.0035 cm^{-1} from 0.0019 cm^{-1}. This reduced resolution (0.0035 cm^{-1}) is appropriate for most studies of atmospheric spectra in the infrared region. For example, the Doppler broadening of ozone lines is larger than 0.004 cm^{-1} in the 3.051 cm^{-1} region of this analysis hence a resolution of 0.0035 cm^{-1} is adequate.

The FTS automatically observes solar absorption spectra 0–10 times a day under clear sky conditions. Since measurements are performed when the solar zenith angle and weather conditions are favorable (giving spectra with adequate precision and noise characteristics), the number of resulting measurement days is about one third of the calendar year. For example, observation days for ozone (3 μm filter) were 107, 101,

ACPD
6, 10299–10339, 2006

EGU

and 93 days for 2001, 2002, and 2003, respectively (see Table 2).

Observed spectral data are automatically transferred from computer storage at Poker Flat, Alaska to the data server in NICT, Tokyo once every 30 min. The System for Alaska Middle-atmosphere Observation data Network (SALMON) is the means of secure and high-speed data transfer experiment; the network comprises a virtual private network (VPN) and the international high-speed Asia Pacific Advanced Network (APAN) system (Oyama et al., 2002). The network system enables the acquisition of spectral data in quasi-real time.

3 Retrieval analysis

The retrieval procedure used the SFIT2 software (version 3.7) algorithm, which incorporates Rodgers' formulation of the Optimal Estimation Method (OEM) with an iterative Newton scheme (Rodgers, 2000). SFIT2 was developed at NASA' s Langley Research Center (LaRC) and the National Institute of Water and Atmosphere (NIWA) (Pougatchev et al., 1996; Pougatchev et al., 1995; Rinsland et al., 1998).

The retrieved height profile $\boldsymbol{x}$ is derived from Eq. (5.10), of Rodgers (2000),

$$\boldsymbol{x}_{i+1} = \boldsymbol{x}_a + \mathbf{G}_y([\mathbf{y} - \mathbf{F}(\boldsymbol{x}_i, \mathbf{b})] + \mathbf{K}_i[\boldsymbol{x}_i - \boldsymbol{x}_a]) \,. \quad (1)$$

where $\boldsymbol{x}$ is the vector containing the profile of chemical species to be retrieved. $\boldsymbol{x}_a$ is the vector of a priori vertical profiles of the chemical species to be retrieved, $\mathbf{y}$ is the vector of the spectral measurements, and F(x, b) is the forward model calculation of the spectrum using model parameters $\mathbf{b}$. The m × n matrix $\mathbf{K} = \frac{\partial \mathbf{F}}{\partial \boldsymbol{x}}$ is a weighting function, which is a measure of the forward models sensitivity to the vector of the chemical species of interest. i is an iteration number.

$\mathbf{G}_y$ is the contribution function matrix:

$$\mathbf{G}_y = \mathbf{S}_a\mathbf{K}_i^T(\mathbf{K}_i\mathbf{S}_a\mathbf{K}_i^T + \mathbf{S}_\epsilon)^{-1} \,. \quad (2)$$

where $\mathbf{S}_\epsilon$ and $\mathbf{S}_a$ are covariance matrices of the measurement noise and a priori vertical profile, respectively. The averaging kernel matrix, $\mathbf{A}$, is given by

$$\mathbf{A} = \mathbf{G}_y \mathbf{K} . \quad (3)$$

The parameters used in the retrieval procedure, including the frequency region, interfering molecules, and diagonal values of the measurement and a priori profile error covariance matrices ($\mathbf{S}_a$ and $\mathbf{S}_\epsilon$) are listed in Table 3. We used the frequency region of ~3051 cm^{-1} for ozone, which is similar to the region used in Seki et al. (2002), because the temperature dependence of these transitions is relatively small and while the only interfering molecules are the wings of two water lines. The microwindow region selected for the HCl and HF retrievals were based on similar regions from Liu et al. (1996). Diagonal elements of $\mathbf{S}_\epsilon$ were taken to be covered 1-σ from the random noise of the observed spectra within the fitted spectral regions.

The instrument line shape (ILS) function was obtained from retrieval using spectrum of HBr cell measurement. A priori profiles were compiled from satellite data. Monthly profiles of ozone, HCl, and HF were calculated by interpolating on both time and vertical grids from HALOE version 19 data between 60–70° N for the time period from 2001 to 2003. Monthly HNO_3 a priori profiles were computed from MLS version 5 data in 1996 using a similar method employed on ozone. The corresponding monthly a priori error covariance matrices, $\mathbf{S}_a$, were determined from the variability of profiles within the monthly set of satellite data used to make the a priori profiles. Of the interfering molecules that affect the various retrieval intervals, H_2O should be treated with care as it is almost always present in all microwindows, to varying degrees. A priori profiles of H_2O were taken from rawinsonde observations made at Fairbanks every day at 15:00 AKST over the range 0–10 km and connected smoothly to a profile above 10 km that was based on model calculations made by the Rutherford Appleton Laboratory (Reburn et al., 1999). The spectral absorption line shape also depends on temperature. Temperature and pressure data were also taken from the same daily 15:00 AKST rawinsonde observations at Fairbanks from 0 to 30 km, and smoothly con-

nected to the nearest UK Meteorological Office (UKMO) point for Poker Flat from 30–50 km, and CIRA86 data for the upper region from 50–100 km (Lorenc, 2000; Swinbank and O'Neill, 1994). The spectroscopic parameters were taken from the High-resolution Transmission (HITRAN) 2004 database (Rothman et al., 2005). Retrieval height steps for all species were set using the internal grid spacing of SFIT2 and were 2 km for the first 50 km and 10 km above this to the top of the atmosphere (100 km).

4 Retrievals of O_3, HNO_3, HCl, and HF

Figure 1 shows examples of the observed and calculated spectra, residuals (observed spectrum – calculated one), retrieval profiles, and averaging kernel functions for O_3, HNO_3, HCl, and HF. In all plots, the observed spectra (indicated with "x") are well fitted to the calculated spectra (indicated with solid lines). The averaging kernel plot for ozone indicates that there is good information in the altitude range from 12–35 km. Similarly, the HNO_3 volume mixing ratio profile has reasonable sensitivity from approximately 15 to 30 km. Both HCl and HF have similar spectral features, i.e. a single isolated line, and therefore their averaging kernels indicate good information from ~12 to 35 km. The height resolutions of the retrieved profiles in the lower stratosphere, expressed as the full width at half maximum (FWHM) of individual averaging kernels, are about 6 km for the four species in this study.

Degrees of freedom for signal (DOFS) indicates the number of independent pieces of information in a measurement (Rodgers, 2000), and is calculated from the trace of the averaging kernels matrix, **A**. Barret et al. (2005) obtained a number of independent partial columns by using the DOFS as a guide. They concluded that in the case of an HCl and HF measurement, one obtains two relatively independent pieces of information that can be approximated by intervals from 14–24 and 24–40 km. For this study, we used a similar procedure; we computed DOFS over altitude ranges to determine the best combination of intervals for the Poker Flat measurement system, i.e., the intervals which match the ones originally obtained by Barret et al. (2005).

For ozone, Barret et al. (2002; 2003) reported a DOFS of 3.0 and 4.7 from retrievals obtained by ground-based FTS for narrow and broad microwindows, respectively. Typical DOFS from the microwindows for the ozone, HNO_3, HCl, and HF retrievals used in this study are 3.0–4.0, 2.0–4.0, 2.0–3.0, and 2.0–3.0, respectively. The values are comparable with Barret et al. (2005, 2002, 2003) and indicate that the vertical resolution of the retrievals from the ground-based FTS spectra used in this study is appropriate for stratospheric investigation.

5 Error analysis

5.1 Theoretical basis

The total retrieval error covariance matrix (**S**) can be expressed as the sum of the error covariance matrices with respect to the contributions from (1) the measurement error due to statistical measurement noise ($\mathbf{S}_M$), (2) the smoothing error, here arising from the limited altitude resolution of the observation system ($\mathbf{S}_N$), and (3) the error due to uncertainties of non-retrieved forward model parameters ($\mathbf{S}_{\text{model}}$), such as spectroscopic parameters:

$$\mathbf{S} = \mathbf{S_M} + \mathbf{S_N} + \mathbf{S_{model}} . \quad (4)$$

The individual terms in Eq. (4) are: 1. measurement error covariance $\mathbf{S}_M$:

$$\mathbf{S_M} = \mathbf{G_y} \mathbf{S}_\epsilon \mathbf{G_y^T} . \quad (5)$$

2. smoothing error covariance $\mathbf{S}_N$:

$$\mathbf{S_N} = (\mathbf{A} - \mathbf{I}) \mathbf{S_a} (\mathbf{A} - \mathbf{I})^\mathbf{T} . \quad (6)$$

3. model parameter error covariance $\mathbf{S}_{\text{model}}$:

$$\mathbf{S_{model}} = (\mathbf{G_y K_b}) \mathbf{S_b} (\mathbf{G_y K_b})^\mathbf{T} . \quad (7)$$

$\mathbf{S}_b$ is the error covariance matrix for the model parameter vector, and $\mathbf{K}_b$ is the weighting function with respect to the model parameters.

5.2 Model parameters

We have estimated the random and systematic errors for the ozone, HNO_3, HCl, and HF retrievals. As well as estimating the errors for total columns, errors for partial columns were also computed. The altitude ranges over which the partial column were derived, and therefore the error estimates, were determined on the basis of the DOFS as discussed in Sect. 4. Barret et al. (2002, 2003) selected five height intervals to compute their partial columns for ozone and error estimations, producing averaging kernel functions that were relatively uncorrelated, as illustrated in Fig. 2a. Connor et al. (1997) first reported the possibility of retrieving several HNO_3 partial columns. Figure 2b shows the averaging kernel functions for HNO_3. In this study, we have adopted the same vertical grids for partial columns as used by Barret et al. (2002, 2003) and Connor et al. (1997) for ozone and HNO_3, respectively. The grids for HCl and HF (see Sect. 4) were selected by using a DOFS that produced averaging kernel functions that were as uncorrelated as possible. These averaging kernel functions (Figs. 2c–d) show large peak values around the center altitudes of the selected layers, although the upper layer, from 20 to 40 km, does not have an obvious Gaussian tail at higher altitudes. However, the two partial columns do separate the stratosphere into two relatively independent layers that give reasonable estimates of both the partial columns and their associated errors.

The total error of the retrieval consists of random and systematic error components. In this analysis, the random error of the retrieval is calculated using Eqs. (5)–(7). Measurement and smoothing errors were computed using formulas (5) and (6). The model parameter temperature error was estimated as a source of non-negligible random error using Eq. (7). The contribution function for temperature was computed by systematically perturbing the forward model over each height layer. SFIT2 is de-coupled from the ray-tracing algorithm, which means that computation of analytical derivatives for temperature is not possible. The temperature error covariance matrix was obtained by computing the standard deviation of temperature from 1 year of temperature data.

ACPD
6, 10299–10339, 2006

EGU

Systematic spectroscopic errors (line strength and pressure broadening parameters) and the Effective Apodization Parameter (EAP) were estimated, because these errors can directly affect retrieved profiles (Barret et al., 2002, 2003; Park, 1982). A simple method of perturbation was used whereby the departure of the retrieved profile with a modified model parameter is calculated from one with an unchanged parameter using formula (8).

$$\mathbf{\Delta x}_{\text{model}} = \mathbf{G_y}[\mathbf{F}(\mathbf{x}, \mathbf{b} + \mathbf{\Delta b}) - \mathbf{F}(\mathbf{x}, \mathbf{b})] \,. \quad (8)$$

Here, Δ b is the uncertainty in the model parameter to be investigated. We assumed uncertainties of 5% higher line strength and 10% smaller air-broadening coefficient in the HITRAN 2004 spectroscopic parameters, on the basis of values described in the error flags of the HITRAN database. The synthesized spectra were therefore calculated with line intensities of all target molecules in the retrieval ranges multiplied by 1.05. These synthesized spectra were then retrieved with unperturbed spectroscopic parameters, as Barret et al. (2002, 2003) did. The same procedure was used for the estimation of error in the air broadening coefficient uncertainty of the target species. The synthesized spectra were calculated with the air-broadening coefficients of all the target molecules in the retrieval ranges multiplied by 0.90 and retrieved with unperturbed parameters. A 10% uncertainty was assumed for the EAP, which is consistent with recent practice (Barret et al., 2002, 2003; Nakajima et al., 1997). The error due to the uncertainty in EAP was calculated with the same method as was used for the spectroscopic parameters. Synthesized spectra were computed with an EAP of 0.9, and then retrieved with an assumed EAP of 1.0.

5.3 Results of error analysis

The results of the error analysis are detailed in Table 4. Twenty measurements were randomly selected, one per month, from 2001 to 2003 to estimate the errors. All error estimates in Table 4 are averages over the 20 randomly selected days. Total random error was calculated as the root-sum-square of the temperature uncertainty, measure-

ment error, and smoothing error. Total systematic errors were calculated as the sum of spectroscopic error and EAP uncertainties.

The errors for the total column and for the partial columns (0–12, 12–18, 18–24, 24–40 km) for ozone were 5.3, 7.2, 6.7, 9.0, and 10.9%, respectively, as recorded in Table 4a. Among the estimated error elements, the impact of temperature uncertainty is small for all the columns. Systematic errors for total and partial columns were –5.2 and –10.5–2.7%, respectively, and these have large variations depending on the partial column. Barret et al. (2002, 2003), as mentioned, estimated the ozone error by using a similar method to this study. Since this study's error estimates are comparable to the ones reported by Barret et al. (2002, 2003) for the narrow window cases, the ozone retrieval process of this study is sound.

The total HNO_3 errors for the total column, 10–20, and 20–30 km partial columns, are 3.4, 11.5, and 9.6%, respectively (Table 4b). A random error of 3.6% was estimated by Rinsland et al. (2000) for both the 14–20 km and 20–50 km HNO_3 partial columns. Systematic errors were reported as 11.4 and 14.2% for the 14–20 km and 20–50 km partial columns, respectively. A direct comparison of the errors from this study with those of Rinsland et al. (2000) is difficult due to differences in the methods used to estimate the errors; however, the error budgets for HNO_3 are consistent between these studies.

The error budgets for HCl and HF are shown in Tables 4c and d. The total HCl errors for the total column, 10–20, and 20–40 km partial columns are 5.9, 5.5, and 11.3%, respectively. The respective total HF errors for the total column, 10–20, and 20–40 km partial columns are 5.3, 4.8, and 10.6%, respectively. Although the errors for HCl and HF are slightly higher than the values reported by Barret et al. (2005), the error estimates from their work and our study are consistent.

When the error budgets for all the reported species are considered, the systematic errors are larger than random errors. Uncertainties in the spectroscopic parameters have the largest impact on the total error. This reflects the direct influence that these types of error have on the spectral line shape in the retrieval process. In summary,

ACPD
6, 10299–10339, 2006

the total errors are within 5.9% for the total column, and 11.5% for the partial columns from the Poker Flat ground-based FTS measurements of stratospheric O_3, HNO_3, HCl, and HF. These errors are consistent with error budgets reported in previous FTS measurements from other NDACC sites, e.g., that of Barret et al. (2005, 2002, 2003) and Rinsland et al. (2000).

6 Validation

6.1 Comparison of FTS O_3 and ozonesonde data

In this section, we validate retrieved ozone data from the gb-FTS measurements by comparison with ozonesonde data. Figure 3 compares the FTS retrieved ozone profiles and ozonesonde profiles. Ozonesonde measurements were performed as a part of the TOMS3-F campaign in Fairbanks (64.81° N, 147.86° W; ∼40 km southwest of Poker Flat) during the spring of 2001, in which 28 profiles were obtained from 20 March to 25 April. The reported error in the ozone profiles from the ozonesonde was approximately 5% (Komhyr et al., 1995).

Profiles whose observation time was within 12 hours of the ozonesonde observation time were selected from the FTS measurement during spring 2001. There were 11 FTIR profiles that had ozonesonde counterparts, whereas there were 2 FTIR profiles with residual root mean squares larger than 1.0%, which indicated a small oscillation in the lower stratosphere, and hence, these two profiles were discarded from the comparison. There were 13 comparisons between FTS and ozonesonde using 9 FTS profiles for 5 days (some FTS profiles had multiple ozonesonde profiles for comparison): 22 March (2 cases), 23 March (6 cases), 24 March (2 cases), 24 April (1 case), and 25 April (2cases) 2001. Figures 3a–d compare minimum time differences for the 22, 23, and 24 March, and 25 April 2001.

When comparing two different measurement techniques that are measuring a similar geophysical quantity, (FTS and ozonesonde profiles), care should be taken when

evaluating the observations systems. In particular, the characteristics of how the measuring systems sample the atmosphere must be taken into account through the use of averaging kernel functions (Rodgers and Conner, 2003). In this study therefore, the profiles observed by the ozonesondes were smoothed with the FTS averaging kernels and these modified ozonesonde profiles were compared with the ozone profiles derived from the FTS. The smoothing procedure is reported in an earlier paper (Yamamori et al., 2006).

Figure 3 compares the smoothed profiles of ozonesonde ozone (pink lines) with FTS ozone profiles. The smoothed profiles have much better agreement with the FTS profiles particularly in Figs. 3b and c for the lower and middle stratosphere.

The percentage differences between FTS ozone and ozonesonde ozone were calculated for 13 comparisons using $100 \times (O_3(\mathrm{FTS}) - O_3(\mathrm{sonde}))/ O_3(\mathrm{sonde})$ %. Figure 4 shows median, 25 percentile, and 75 percentile values of the differences. The blue dashed lines are computed error ranges for the partial columns. From 15 to 30 km, the median of the difference is within the error range of the FTS partial column. There is about a 50% median difference with large scatter at 7 km. This large difference is caused by a combination of limited sensitivity from the retrieval (as the averaging kernel rapidly falls off around this altitude), and the effect this has on our choice of the a priori profile in the troposphere. This latter effect is due to the limited sensitivity of the mean HALOE profile below the tropopause. This problem is further exacerbated by the rapid spatial (vertical) and temporal change in ozone mixing at and below the tropopause. Note that the error inherent in a profile is larger than the error in a partial column. The error in the ozonesonde profile is not considered in the error ranges.

Generally, the consistency of the profiles (gb-FTS and ozonesonde) in the lower and middle stratosphere, where most of the ozone exists, verifies that the observations by the Poker Flat FTS and retrieval method for ozone is comparable with previously reported work (Barret et al., 2002, 2003).

ACPD
6, 10299–10339, 2006

6.2 Comparison of FTS O_3 and TOMS data

Figure 5 compares the ozone total column from the FTS and Earth-Probe Total Ozone Mapping Spectrometer (TOMS) version 8 data from 2001 to 2003. The FTS retrieved ozone total column is shown with error bars estimated from the error analysis in Sect. 5 (5.3%). The FTS and EP-TOMS measurements are consistent in terms of seasonal trends; however, there is a uniform small negative bias in the EP TOMS data. The time series of the two data sets does show similar small-scale features on time scales of several tens of days.

One factor that explains some of this bias concerns a calibration error in TOMS. As reported in TOMS News (http://toms.gsfc.nasa.gov/news/news.html), there is a –2% to –4% error in TOMS at 50 degrees latitude, with the bias being slightly higher in the northern hemisphere than in the southern hemisphere. There is no indication in the literature of this bias error at 65° N, but if a 5% bias in TOMS is assumed, the resultant difference between FTS and TOMS data is reduced as shown by the blue symbol in Fig. 6, with many data points coming within the error range of the one-to-one line.

The large departures from this one-to-one line that still remain are possibly explained by spectroscopic uncertainties. Using the HITRAN 2004 spectroscopic parameters for the FTS retrieval instead of HITRAN 2000 introduces systematic differences between the FTS retrieved ozone and EP-TOMS data. The five strongest lines (intensities) of ozone in the retrieval microwindow from the HITRAN 2004 data (3051.3800, 3051.8307, 3051.4742, 3051.7555, and 3051.3068 cm^{-1}) are about 4% lower than the respective HITRAN 2000 lines. Large differences in the air broadening coefficient and temperature dependencies of the half widths between HITRAN 2004 and the earlier HITRAN 2000 values were reported by Rinsland et al. (2003). Differences of up to 10% exist in the broadening coefficients of the two HITRAN databases. If these discrepancies are considered, the uncertainty in the spectroscopic parameters are potentially one of the largest error sources in the budget analysis of Sect. 5. If an additional ~5% bias is assumed for spectroscopic parameter bias, almost all the data now falls within

ACPD
6, 10299–10339, 2006

the error range of the one-to-one line (Fig. 6).

6.3 Comparison of FTS O_3, HCl, and HF with HALOE data

In this section, we compare stratospheric columns of O_3, HCl, and HF derived from measurements made by the HALogen Occultation Experiment (HALOE) onboard the UARS satellite with data from the gb-FTS measurements. An overview of HALOE observations is given in Russell-III et al. (1993). Errors in HALOE derived O_3 were reported to be 8–30% from 1 to 100 hPa, and thus, the HALOE O_3 data are within the error range of correlative measurements (Bruhl et al., 1996). The total error for the HALOE HCl columns was reported to be from 12–24% throughout the stratosphere (Russell-III et al., 1996a). Russell-III et al. (1996a) reported that HALOE HCl measurements tend to be low (from 8 to 20%) in correlative comparisons with other instruments. Total errors for HALOE HF are reported to be 14–27%, depending on the altitude in the stratosphere (1–100 hPa) (Russell-III et al., 1996b).

Figure 7 shows stratospheric columns (17 to 45 km) of ozone, HCl, and HF for gb-FTS and HALOE version 19 over the time period from 2001 to 2003. The error ranges of the FTS O_3, HCl, and HF partial columns in Fig. 7 are the ones for altitude ranges 18–24, 20–40, and 20–40 km, respectively. Plotted are HALOE data within 10°latitude and 20°longitude of Poker Flat. HALOE data from this selected area roughly correspond to the Alaskan location. Time series of the chemical species from HALOE and the gb-FTS were fitted using functions that include a seasonal cycle and annual trend term as shown in the figure. The seasonal variation of the HALOE and FTS ozone, HCl, and HF columns are reasonably consistent for the 2001–2003 period, although the FTS data are uniformly higher than the HALOE data.

For a detailed comparison, Fig. 8 shows scatter plots of ozone, HCl, and HF columns for the HALOE and FTS datasets measured on the same day for the 2001–2003 time period. The FTS O_3 columns, Fig. 8a, correlate well with HALOE data (r=0.89). Average relative differences calculated with the relation (O_3(FTS)-O_3(HALOE))/O_3(HALOE) are about 12%. McHugh et al. (2005) reported FTS ozone measurements of the At-

mospheric Chemistry Experiments (ACE) that were about 0.4 ppmv larger than those of the HALOE version 19 derived ozone mixing ratio in the altitude range from 35 to 70 km. This study's comparison of HALOE and gb-FTS data indicated a similar bias. If the bias of McHugh et al. (2005) is considered, most of the measurements fall within the indicated error ranges in Fig. 8a.

Figure 8b shows the FTS HCl correlation plot with HALOE from 2001 to 2003, and this plot also indicates a positive bias for the FTS data. The HALOE–FTS correlation (r=0.54) is lower than ozone (r=0.89) as ozone is driven by a much larger seasonal cycle.

In a similar fashion to ozone, the average relative difference for HCl, calculated as (HCl(FTS)-HCl(HALOE))/HCl(HALOE), is again about 12%. A similar bias between HALOE data and correlative measurements was reported by Russell III et al. (1996a). Liu et al. (1996) reported that HCl profiles from gb-FTS agree with HALOE data within the combined error limit, but are 5 to 20% higher than the HALOE values. McHugh et al. (2005) also reported that ACE-FTS HCl values are 10–20% higher than those of HALOE version 19 between 20 and 48 km.

In Fig. 8c, the HF columns measured by FTS are 9% larger than those of HALOE HF. The ACE-FTS derived HF profiles indicate 10–20% larger values than HALOE profiles throughout the stratosphere (McHugh et al., 2005). There is a moderate correlation (r=0.65) between the two measurements.

Overall, the gb-FTS O_3, HCl, and HF stratospheric columns are well correlated but are about 10% higher than the HALOE version 19 columns. However, the two measurements are consistent if the bias reported by Russell III et al. (1996a), Liu et al. (1996), and McHugh et al. (2005) is considered. The two measurements, Poker Flat FTS and HALOE, will be compared in the future after HALOE data has been updated with the new version (McHugh et al., 2005).

ACPD
6, 10299–10339, 2006

7 Seasonal variations of O_3, HNO_3, HCl, and HF from 2001 to 2003

Figures 9a–d are time-height cross sections (upper panel) and the columns (lower panel, see Fig. 9 caption for details) of O_3, HNO_3, HCl, and HF from 2001 to 2003. The height-time cross sections are plotted for the altitude range from 10–50 km, where the chemical species were retrieved with good vertical information. Blank areas represent either no measurement or data that were rejected on the basis of quality control criteria (for example, signal to noise ratio). Intensive measurements are made from spring to autumn by the Poker Flat FTS system every year, whereas few measurements or few data with high enough precision are gathered during winter when the solar zenith angle is large (sun at or below the horizon). The profiles selected to produce Fig. 9 comprised 210, 160, 228, and 194 profiles for ozone, HNO_3, HCl, and HF, respectively.

Despite the limited vertical resolution inherent in the FTS profiles, the retrieved profiles do exhibit seasonally varying features for the chemical species selected in this study. In the upper panel of Fig. 9a, the ozone mixing ratio over Poker Flat shows large seasonal variations, with the maximum ratio occurring around 38 km as expected. Low ozone mixing ratios, indicated in purple at low altitudes, gradually ascend towards the end of the season. Ozone total columns (the black diamonds in the lower panel of Fig. 9a) have a seasonal dependence, with their maximum value occurring in late winter or spring and minimum in summer. The time series of the ozone partial columns indicate that the seasonal cycle observed in the total column is mainly driven by changes in the lower stratosphere (12–18 and 18–24 km), with less seasonal dependence in the 0–12 km and 24–40 km partial columns. The largest seasonal change in ozone mixing ratio occurs at altitudes different from the ones where the largest seasonal change in the column happens, which is expected for ozone.

Figure 9b is the retrieved time-height cross-section and columns for HNO_3. The maximum mixing ratio for HNO_3 occurs in the lower stratosphere, as expected. Year-to-year variability of the HNO_3 total column is larger than that of ozone. The high abundance for the HNO_3 total column of around 3×10^{16} molecules cm^{-2} in spring gradually decreases

towards summer and increases again in autumn. This is consistent with summer photodissociation. Seasonal changes in the HNO_3 column occur at 10–20 km range, as shown by the blue symbols in Fig. 9b, with notable changes occurring in the spring of 2002. The increase in the HNO_3 total column during the fall of 2001 appears to be driven by changes occurring at 20–30 km. As in the case of ozone, the altitude regions with the largest seasonal changes in mixing ratio are different from the altitudes of the largest changes in the HNO_3 columns.

Figures 9c and d are the retrieved time-height cross-section (upper panel) and columns (lower panel) for HCl and HF, respectively. The mixing ratio profiles of these two species have similar shapes; that is, these mixing ratios gradually increase with altitude from the stratosphere to higher altitudes. Both HCl and HF have similar seasonal cycles to those of O_3 and HNO_3 over the time period of the data (2001 to 2003). These seasonal cycles in HCl and HF occur in the 10–20 km range as shown in the figures. HF has a larger partial column at 20–40 km (red symbols) than at 10–20 km (blue symbols). There are also possible dynamical features in the 10–20 km column, particularly for HF, that are also apparent in the HNO_3 10–20 km column. This is quite clear for the 2002 data. The work to evaluate these dynamics is ongoing.

8 Summary

We have been observing stratospheric minor species over Poker Flat, Alaska since 1999 by using a high-resolution FTS. Poker Flat is at an interesting location between the Arctic and mid-latitudes. To investigate the behavior of stratospheric ozone and ozone-related species, vertical profiles of ozone, HNO_3, HCl, and HF for the period of 2001–2003 were retrieved using Rodgers' formulation of the Optimal Estimation Method (OEM). The averaging kernels functions indicated that the four chemical species were retrieved with the highest information content in the lower stratosphere. Due to the limited vertical resolution inherent in gb-FTS measurements, there are only 2 to 4 relatively independent partial columns that can be investigated, depending on

gas species.

The retrieval errors were estimated in detail and used as the basis for discussion of seasonal and inter-annual variability in stratospheric ozone and ozone-related species. The random and systematic errors of the retrieved partial column of the chemical species were calculated by formal error analysis. The total ozone errors for the total column and 4 partial independent columns are 5.3% and 6.7–10.9%, respectively. Similarly, the total errors for the HNO_3, HCl, and HF total columns were 3.4, 5.9, and 5.3% respectively, while the total errors for the reported two partial columns of HNO_3, HCl, and HF were 9.6–11.5, 5.5–11.3, and 4.8–10.6 % , respectively. These errors are consistent with previous error budgets of the FTS measurements reported from other NDACC sites. In our analysis, line parameters and EAP uncertainties were significant components of the total error.

We validated the data retrieved from our FTS measurements by comparison with ozonesonde, Earth-Probe TOMS, and HALOE data. For consistency with current best practice, the ozonesonde profiles were smoothed by the FTS averaging kernel functions. These smoothed profiles agreed well with the FTS ozone profiles within their calculated error ranges. The total column ozone observed by the FTS and EP-TOMS version 8 were consistent within the FTS error bars if the known systematic bias in the EP-TOMS data and HITRAN 2004 is taken into account.

Stratospheric columns of ozone, HCl, and HF observed by the FTS were compared with HALOE version 19 data. The FTS O_3, HCl, and HF stratospheric columns correlated well with HALOE data but were about 10% high. However, the two measurements are consistent when the biases reported by other studies are taken into account. A new version of HALOE has been developed, and we will compare the two measurements again by using the updated data (McHugh et al., 2005). FTS HNO_3 profiles during the 2003 spring agreed well with the Improved Limb Atmospheric Spectrometer (ILAS) II data (Yamamori et al., 2006).

Of the height-time cross-sections of the chemical species retrieved by FTS in this study, the ozone data from 2001–2003 exhibited a seasonal cycle with its maximum

mixing ratio being in the mid-stratosphere. HNO_3 also exhibits a seasonal cycle with its maximum mixing ratio being in the lower stratosphere. All four retrieved species had similar seasonal cycles, while seasonal variations in the columns of the all species occurred in the lower stratosphere.

This study is the first report of retrieval results with a detailed formal error analysis of stratospheric molecules above the Poker Flat FTS observation site. A further investigation of the ozone loss mechanisms over Poker Flat will be reported in the near future.

Acknowledgements. The authors thank the United Kingdom Meteorological (UKMO) Office for supplying temperature and pressure data for the retrievals. We are grateful to NASA's Goddard Space Flight Center for providing Total Ozone Mapping Spectrometer (TOMS) data from the Earth Probe satellite and HALogen Occultation Experiments (HALOE) data and Microwave Limb Sounder data from the Upper Atmosphere Research Satellite (UARS). The SALMON system which has made an important contribution to automatic observation and transfer of Poker Flat FTS data was developed under Alaska Project, NICT.

References

Barret, B., Maziére, M. D., and Demoulin, P.: Retrieval and characterization of ozone profiles from solar infrared spectra at the Jungfraujoch, J. Geophys. Res, 107(D24), 4788, doi:10.1029/2001JD001298, 2002.

Barret, B., Mazie're, M. D., and Demoulin, P.: Correction to "Retrieval and characterization of ozone profiles from solar infrared spectra at the Jungfraujoch", J. Geophys. Res, 108(D12), 4372, doi:10.1029/2003JD003809, 2003.

Barret, B., Hurtmans, D., Carleer, M. R., Mazie're, M. D., Mahieu, E., and Coheur, P.-F.: Line narrowing effect on the retrieval of HF and HCl vertical profiles from ground-based FTIR measurements, J. Quant. Spectrosc. Radiat. Transfer, 95, 499–519, 2005.

Bruhl, C., Drayson, S. R., Russell III, J. M., Crutzen, P. J., McInterney, J. M., Purcell, P. N., Claude, H., Gernandt, H., McGee, T. J., McDermid, I. S., and Gunson, M. R.: Halogen Occultation Experiment ozone channel validation, J. Geophys. Res, 101(D6), 10 217–10 240, 1996.

Connor, B. J., Jones, N. B., Wood, S. W., Keys, J. G., Rinsland, C. R., and Murcray, F. J.: Retrieval of HCl and HNO_3 profiles from ground-based FTIR data using SFIT2., paper presented at XVIII Quadrennial Ozone Symposium, L'Aquila, Italy, Parco Scientifico e Technologico d'Abruzzio, 1997.

Goldman, A., Paton-Walsh, C., Bell, W., Toon, G. C., Blavier, J.-F., Sen, B., Coffey, M. T., Hannigan, J. W., and Mankin, W. G.: Network for the Detection of Stratospheric Change Fourier transform infrared intercomparison at Table Mountain Facility, November 1996, J. Geophys. Res, 104(D23), 30 481–30 503, 1999.

Hase, F., Hannigan, J. W., Coffey, M. T., Goldman, A., Hopfner, M., Jones, N. B., Rinsland, C. R., and Wood, S. W.: Intercomparison of retrieval codes used for the analysis of high-resolution, ground-based FTIR measurements, J. Quant. Spectrosc. Radiat. Transfer, 87(1), 25–52, 2004.

Komhyr, W. D., Barnes, R. A., Brothers, G. B., Lathrop, J. A., and Opperman, D. P.: Electrochemical concentration cell ozonesonde performance evaluation during STOIC 1989, J. Geophys. Res, 100(D5), 9231–9244, 1995.

Liu, X., Murcray, F. J., Murcray, D. G., and Russell III, J. M.: Comparison of HF and HCl vertical profiles from ground-based high-resolution infrared solar spectra with Halogen Occultation Experiment observations, J. Geophys. Res, 101(D6), 10 175–10 181, 1996.

Lorenc, A. C.: The Met. Office global three-dimensional variational data assimilation scheme, Q. J. Royal Meteorol. Soc., 126, 2991–3011, 2000.

Manney, G. L., Froidevaux, L., Santee, M. L., Zurek, R. W., and Waters, J. W.: MLS observations of Arctic ozone loss in 1996–97, Geophys. Res. Lett., 24(22), 2697–2700, 1997.

McHugh, M., Magill, B., Walker, K. A., Boone, C. D., Bernath, P. F., and III, J. M. R.: Comparison of atmospheric retrievals from ACE and HALOE, Geophys. Res. Lett., 32, L15S10, doi:10.1029/2005GL022403, 2005.

Murayama, Y., Mori, H., Ishii, M., Kubota, M., and Oyama, S.: CRL Alaska Project-International Collaborations for observing Arctic atmosphere environment in Alaska, Journal of the Communications Research Laboratory, 49(2), 143–152, 2003.

Nakajima, H., Liu, X., Murata, I., Kondo, Y., Murcray, F. J., Koike, M., Zhao, Y., and Nakane, H.: Retrieval of vertical profiles of ozone from high-resolution infrared solar spectra at Rikubetu, Japan, J. Geophys. Res, 102(D25), 29 981–29 990, 1997.

Newchurch, M. J., Yang, E.-S., Cunnold, D. M., Reinsel, G. C., Zawodny, J. M., and III, J. M. R.: Evidence for slowdown in stratospheric ozone loss: First stage of ozone recovery, J.

Geophys. Res, 108(D16), 4507, doi:10.1029/2003JD003471, 2003.
Oyama, S., Murayama, Y., Ishii, M., and Kubota, M.: Development of SALMON system and the environmental data transfer experiment, Journal of the Communications Research Laboratory, 49(2), 253–257, 2002.
Park, J. H.: Effect of interferogram smearing on atmospheric limb sounding by Fourier transform spectroscopy, Appl. Opt., 21(8), 1356–1366, 1982.
Paton-Walsh, C., Bell, W., Gardiner, T., Swann, N., Woods, P., Notholt, J., Schutt, H., Galle, B., Arlander, W., and Mellqvist, J.: An uncertainty budget for ground-based Fourier transform infrared column measurements of HCl, HF, N_2O, and HNO_3 deduced from results of side-by-side instrument intercomparisons, J. Geophys. Res, 102(D7), 8867–8873, 1997.
Pougatchev, N. S., Conner, B. J., and Rinsland, C. R.:Infrared measurements of the ozone vertical distribution above Kitt Peak, J. Geophys. Res., 100(D8), 16 689–16 697, 1995.
Pougatchev, N. S., Conner, B. J., Jones, N. B., and Rinsland, C. R.: Validation of ozone profile retrievals from infrared ground-based solar spectra, Geophys. Res. Lett., 23(13), 1637–1640, 1996.
Reburn, W. J., Siddans, R., Kerridge, B. J., Bühler, S. A., Engeln, A. v., Urban, J., Wohlgemuth, J., Künzi, K., Feist, D., Kämpfer, N., and Czekala, H.: Study on upper troposphere/lower stratosphere sounding, Executive summary, ESA Contact No.:12053/97/NL/CN., 1999.
Reinsel, G. C., Miller, A. J., Weatherhead, E. C., Flynn, L. E., Nagatani, R. M., Tiao, G. C., and Wuebbles, J.: Trend analysis of total ozone data for turnaround and dynamical contributions, J. Geophys. Res, 110, D16306, doi:10.129/2004JD004662, 2005.
Rinsland, C. R., Jones, N. B., Conner, B. J., Logan, J. A., Pougatchev, N. S., Goldman, A., Murcray, F. J., Stephen, T. M., Pine, A. S., Zander, R., Mahieu, E., and Demoulin, P.: Northern and southern hemisphere ground-based infrared spectroscopic measurement of tropospheric carbon monoxide and ethane, J. Geophys. Res, 103(D21), 28 197–28 217, 1998.
Rinsland, C. R., Goldman, A., Conner, B. J., Stephen, T. M., Jones, N. B., Wood, S. W., Murcray, F. J., David, S. J., Blatherwick, R. D., Zander, R., Mahieu, E., and Demoulin, P.: Correlation relationship of stratospheric molecular constituents from high spectral resolution, ground-based infrared solar absorption spectra, J. Geophys. Res, 105(D11), 14 637–14 652, 2000.
Rinsland, C. R., Flaud, J.-M., Perrin, A., Birk, M., Wagner, G., Goldman, A., Barbe, A., Backer-Barilly, M.-R. D., Mikhailenko, S. N., Tyuterev, V. G., Smith, M. A. H., Devi, V. M., Benner, D. C., Schreier, F., Chance, K. V., Orphal, J., and Stephen, T. M.: Spectroscopic parameters for ozone and its isotopes: recent measurements, outstanding issues, and prospects for

improvements to HITRAN, J. Quant. Spectrosc. Radiat. Transfer, 82, 207–218, 2003.
Rodgers, C. O.: Inverse methods for atmospheric sounding: Theory and practice, World Scientific, 2000.
Rodgers, C. O. and Conner, B. J.: Intercomparison of remote sounding instruments, J. Geophys. Res, 108(D3), 4116, doi:10.1029/2002JD002299, 2003.
Rothman, L. S., Jacquemart, D., Barbe, A., et al.:The HITRAN 2004 molecular spectroscopic database, J. Quant. Spectrosc. Radiat. Transfer, 96, 139–204, 2005.
Russell-III, J. M., Gordley, L. L., Park, J. H., Drayson, S. R., Hesketh, W. D., Cicerone, R. J., Tuck, A. F., Frederick, J. E., Harries, J. E., and Crutzen, P. J.: The halogen occultation experiment, Journal of Geophysical Research, 98(D6), 10 777–10 797, 1993.
Russell-III, J. M., Deaver, L. E., Luo, M., Park, J. H., Gordley, L. L., Tuck, A. F., Toon, G. C., Gunson, M. R., Traub, W. A., Johonson, D. G., Jucks, K. W., Murcray, D. G., Zander, R., Nolt, I. G., and Webster, G. R.: Validation of hydrogen chloride measurements made by the Halogen Occultation Experiment from the UARS platform., J. Geophys. Res, 101(D6), 10 151–10 162, 1996a.
Russell-III, J. M., Deaver, L. E., Luo, M., Cicerone, R. J., Park, J. H., Gordley, L. L., Toon, G. C., Gunson, M. R., Traub, W. A., Johonson, D. G., Jucks, K. W., Zander, R., and Nolt, I. G.: Validation of hydrogen fluoride measurements made by the Halogen Occultation Experiment from the UARS platform, J. Geophys. Res, 101(D6), 10 163–10 174, 1996b.
Seki, K., Kasai, Y., Murayama, Y., Mizutani, K., Itabe, T., Murcray, F. J., Simpson, W. R., and Lioyd, S. A.: Trace Gas Observation with Poker Flat FTIR, J. Communications Res. Laboratory, 48(2), 171–178, 2002.
Swinbank, R. and O'Neill, A.: A stratosphere-troposphere data assimilation system, Monthly Weather Rev., 122, 686–702, 1994.
World Meteorological Organization (WMO), Scientific Assessment of Ozone Depletion:2002, Global Ozone Research and Monitoring Project-Report No.47, 498 pp, Geneva, 2003.
Wood, S. W., Bodeker, G. E., Boyd, I. S., Jones, N. B., Connor, B. J., Johnston, P. V., Matthews, W. A., Nichol, S. E., Murcray, F. J., Nakajima, H., and Sasano, Y.: Validation of version 5.20 ILAS HNO_3, CH_4, N_2O, O_3, and NO_2 using ground-based measurements at Arrival Heights and Kiruna, J. Geophys. Res, 107(D24), 8208, doi:10.129/2001JD000581, 2002.
Yamamori, M., Kagawa, A., Kasai, Y., Mizutani, K., Murayama, Y., Sugita, T., Irie, H., and Nakajima, H.: Validation of ILAS-II version 1.4 O_3, HNO_3, and temperature data through comparison with ozonesonde, ground-based FTS, and lidar measurements in Alaska, J.

Geophys. Res., 111, D11S08, doi:10.1019/2005JD006438, 2006.

Table 1. Filters, their wavenumber ranges, and detecters used for the FTS measurements at Poker Flat.

Filter	Wavenumber range [cm^{-1}]	Detector
filter 2	4000–4300	InSb
filter 3	2425–3060	InSb
filter 3.5	3000–3750	InSb
filter 4	1975–2550	InSb
filter 5	1850–2175	InSb
filter 6	1550–2125	MCT
filter 9	750–1325	MCT

ACPD
6, 10299–10339, 2006

Table 2. Days of ozone observation (filter 3 : 2425–3060 cm^{-1}) from 2001 to 2003.

Month	1	2	3	4	5	6	7	8	9	10	11	12	Total
2001	0	4	16	17	16	18	13	16	15	2	0	0	107
2002	0	5	19	15	16	15	15	8	5	2	1	0	101
2003	0	5	17	18	20	21	9	0	0	3	0	0	93

Multiple measurements during a day are counted as one measurement.

ACPD
6, 10299–10339, 2006

Table 3. Retrieved molecules, microwindows used for retrievals, including interfering molecules, and diagonal values of $\mathbf{S}_\epsilon$ and $\mathbf{S}_a$ used in calculations.

Molecule	Microwindow [cm^{-1}]	Interfering Molecules	$\mathbf{S}_\epsilon$ †	$\mathbf{S}_a$ ‡ [%]
O_3	3051.290–3051.900	H_2O CH_4 HDO CH_3D	200	15
HNO_3	867.450–869.250	H_2O OCS	200	30
HCl	2925.800–2926.000	H_2O CH_4 NO_2 O_3	200	15
HF	4038.804–4039.148	H_2O	150	15

† $\mathbf{S}_\epsilon$ is the covairance matrix of measurement noise, which is estimated from random noise in the spectral fits.
‡ $\mathbf{S}_a$ is the covariance matrix of a priori information variability. Values are in % of mixing ratio. The same values are used for all altitudes.

Table 4a. Errors in ozone for 0–12, 12–18, 18–24, 24–40 km partial columns and for the total column. All errors are in % of the column amount. DOFS of these partial columns and total column are also indicated.

Altitude [km]	0–12	12–18	18–24	24–40	Total Col.
Temperature Uncertainty	0.8	0.9	1.2	1.0	0.3
Measurement Error	4.2	3.1	2.4	1.2	0.6
Smoothing Error	5.2	5.8	5.2	2.6	0.4
Total Random Error	6.7	6.6	5.9	3.0	0.8
O_3 Air Broadening Coefficient Uncertainty	6.7	6.7	0.7	–9.0	–0.8
O_3 Line Intensity Uncertainty	–3.9	–4.5	–4.5	–5.2	–4.6
EAP Uncertainty	–0.1	–1.0	–3.0	3.7	0.2
Total Systematic Error	2.7	1.2	–6.8	–10.5	–5.2
Total Errors	7.2	6.7	9.0	10.9	5.3
DOFS	0.5	0.6	0.7	1.2	3.2

A 5% larger line intensity and 10% smaller air-broadening coefficient than those of HITRAN 2004 are assumed for the spectroscopic error.

Table 4b. Error of HNO_3.

Altitude [km]	10–20	20–30	Total Col.
Temperature Uncertainty	0.9	0.8	0.5
Measurement Error	5.7	4.2	2.5
Smoothing Error	9.5	6.4	2.1
Total Random Error	11.1	7.7	3.3
HNO_3 Air Broadening Coefficient Uncertainty	2.7	–1.6	3.4
HNO_3 Line Intensity Uncertainty	–4.7	–5.1	–4.4
EAP Uncertainty	–1.1	1.0	0.0
Total Systematic Error	–3.1	–5.7	–1.0
Total Errors	11.5	9.6	3.4
DOFS	0.7	1.1	2.6

ACPD
6, 10299–10339, 2006

Table 4c. Error of HCl.

Altitude [km]	10–20	20–40	Total Col.
Temperature Uncertainty	0.6	0.5	0.4
Measurement Error	3.2	1.7	1.2
Smoothing Error	3.6	2.7	1.4
Total Random Error	4.9	3.3	1.9
HCl Air Broadening Coefficient Uncertainty	3.1	–7.3	–1.7
HCl Line Intensity Uncertainty	–4.2	–5.3	–4.0
EAP Uncertainty	–1.4	1.8	0.1
Total Systematic Error	–2.5	–10.8	–5.6
Total Errors	5.5	11.3	5.9
DOFS	0.8	1.2	2.1

Table 4d. Error of HF.

Altitude [km]	10–20	20–40	Total Col.
Temperature Uncertainty	0.8	0.6	0.4
Measurement Error	3.1	1.3	0.9
Smoothing Error	3.5	2.3	0.5
Total Random Error	4.7	2.7	1.1
HF Air Broadening Coefficient Uncertainty	6.4	–6.2	–0.9
HF Line Intensity Uncertainty	–4.2	–5.4	–4.5
EAP Uncertainty	–1.4	1.4	0.2
Total Systematic Error	0.8	–10.2	–5.2
Total Errors	4.8	10.6	5.3
DOFS	0.8	1.1	2.1

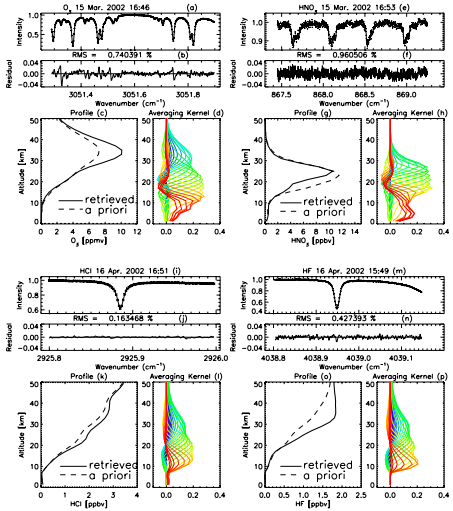

Fig. 1. **(a)** Superimposition of observed and fitted normalized spectra for ozone. The fitted example is for an observation on 15 March 2002 at 16:46 (AKST). SZA=79. Observed and calculated spectra are indicated with a cross mark and solid line, respectively. **(b)** Residual of these spectra. The residual is calculated by observed – calculated spectrum. Residual root mean square is 0.74% of the intensity. **(c)** Ozone profiles from 0 km to 50 km retrieved from the spectrum of Fig. 1a. Solid line shows a retrieved profile. Long-dashed line is a priori vertical profile. **(d)** Averaging kernel function for the ozone mixing ratios. **(e)**–**(h)** are the same as (a)–(d), except for nitric acid. This spectrum was observed on 15 March 2002 at 16:53 (AKST). SZA=79. **(i)**–**(l)** are the same as (a), except for HCl. Spectrum was observed on 16 April 2002 at 16:51 (AKST). SZA=68. **(m)**–**(p)** are the same as (a), except for HF. HF spectrum was observed on 16 April 2002 at 15:49 (AKST). SZA=63. If the residual was larger than a preselected threshold (for example, 1.5% of the root-mean-square residual was selected for ozone), this data was removed from the plot and not included in the consideration of seasonal variations or correlations.

ACPD
6, 10299–10339, 2006

EGU

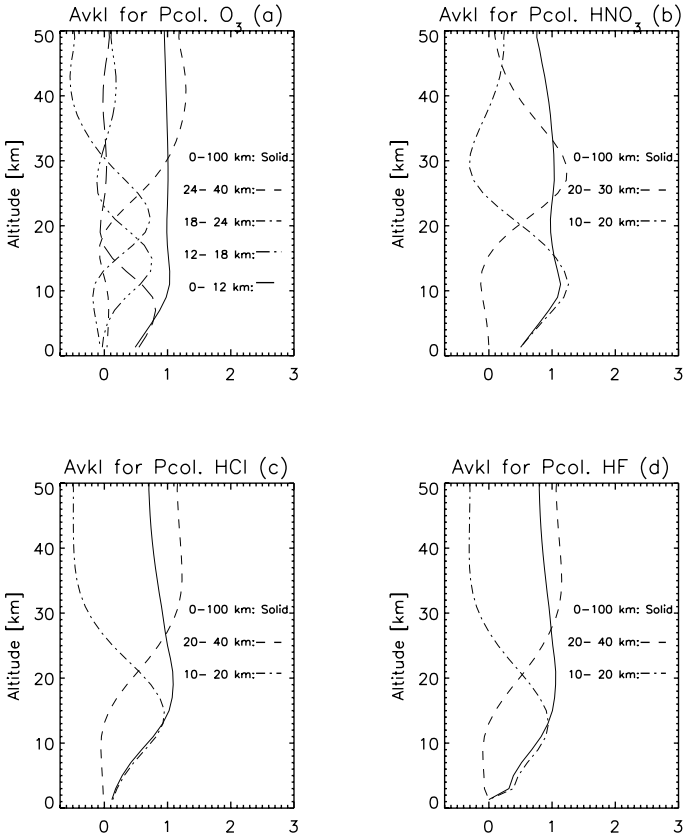

Fig. 2. (a) Averaging kernel functions for partial columns of ozone. Averaging kernel functions for 0–12, 12–18, 18–24, and 24–40 km are shown as independent layers. The total column is also indicated as a solid line. **(b)**, **(c)**, and **(d)** are plots of HNO_3, HCl, and HF, respectively. The averaging kernels are calculated using the same spectra used for Fig. 1.

ACPD
6, 10299–10339, 2006

EGU

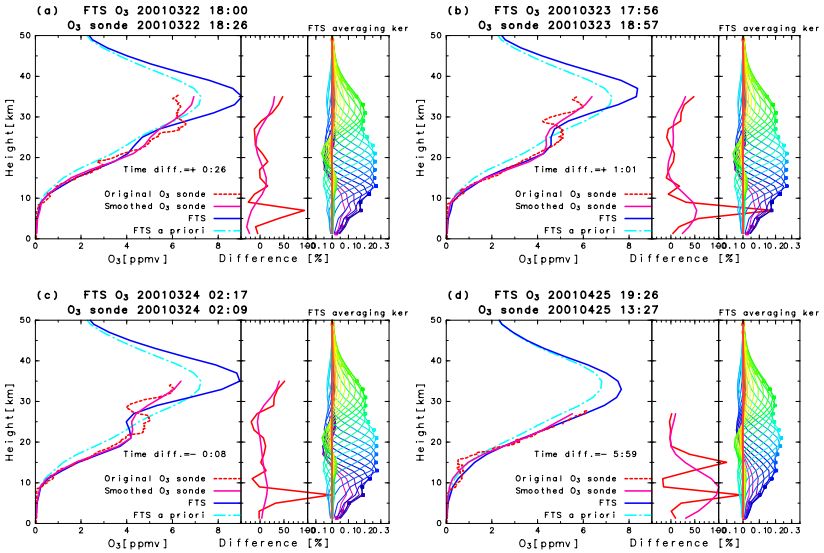

Fig. 3. **(a)** (left) Comparison of ozone profiles measured by FTS with colocated ozonesonde measurements from 0 to 50 km. The solid blue line shows a retrieved ozone profile on 22 March 2001 18:00 UTC. The dash-dotted sky-blue line is the a priori profile used for this retrieval. The dotted red line shows a profile observed by an ozonesonde launched from Fairbanks (64.81° N, 147.86° W) on 22 March 2001 18:26 UTC. The pink solid line shows an ozonesonde profile smoothed using the FTS averaging kernel. The time difference between the ozonesonde and FTS measurements is indicated in the figure (ozonesonde observation time – FTS observation time). (middle) Red line is the relative difference between the original ozonesonde and FTS ozone as calculated by $100\times(O_3(\mathrm{FTS})\text{-}O_3(\mathrm{sonde}))/O_3(\mathrm{sonde})$. The pink line is the relative difference between the smoothed ozonesonde and FTS ozone calculated with the same method as the original ozonesonde difference above. (right) An averaging kernel function for the FTS measurement of (a), which is used to smooth the ozonesonde profile. **(b)–(d)** are the same as (a), except for the measurements by FTS and ozonesonde on 23 March, 24 March, and 25 April.

ACPD
6, 10299–10339, 2006

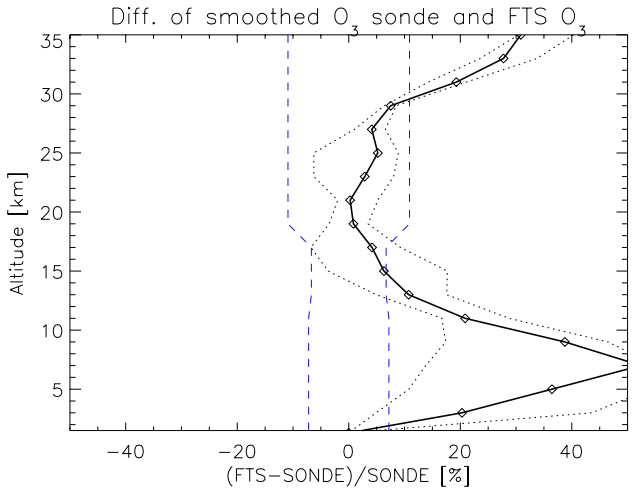

Fig. 4. Difference between ozonesonde ozone profiles observed in Fairbanks (64.81° N, 147.86° W; ~40 km southwest of Poker Flat) and FTS ozone profiles during the spring of 2001. FTS observations whose RMS residuals are smaller than 1% and observation time is within 12 h of the ozonesonde observations were selected for the comparison. Open diamond with solid line shows the median of the relative differences calculated from the 13 comparisons selected according to the criteria. Black dotted lines are the 25 and 75 percentile values. Blue dashed line is the FTS error range of the partial column calculated by the error analysis at the corresponding altitude.

ACPD
6, 10299–10339, 2006

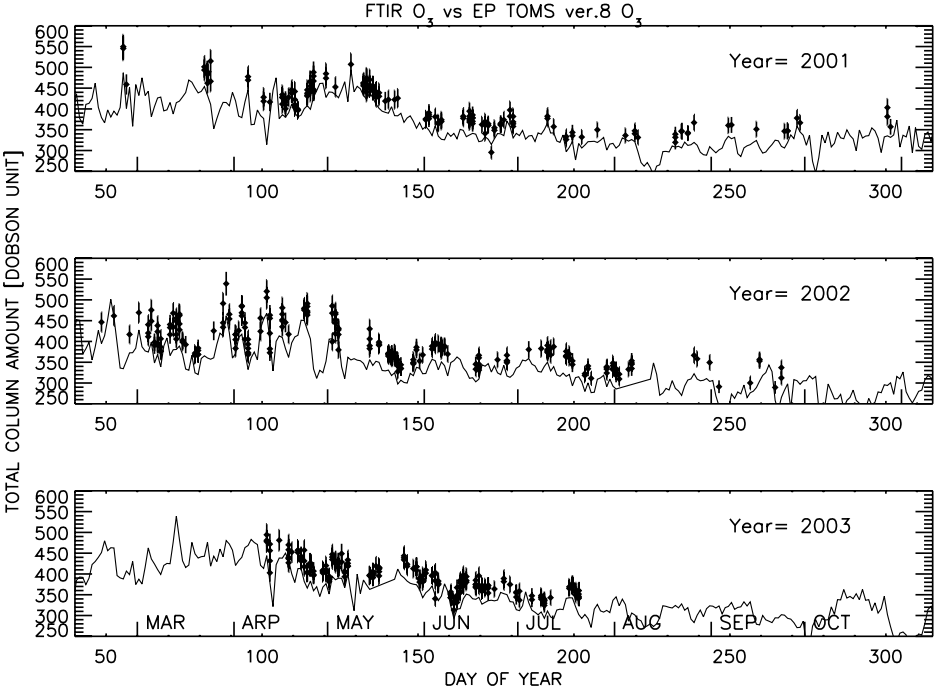

Fig. 5. Comparison of FTS ozone and Earth-Probe TOMS data. Filled diamonds with error bars indicate FTS ozone. The error bar for the FTS ozone data is taken from the total error as computed in the error analysis. The solid line is EP-TOMS data over Poker Flat.

ACPD
6, 10299–10339, 2006

EGU

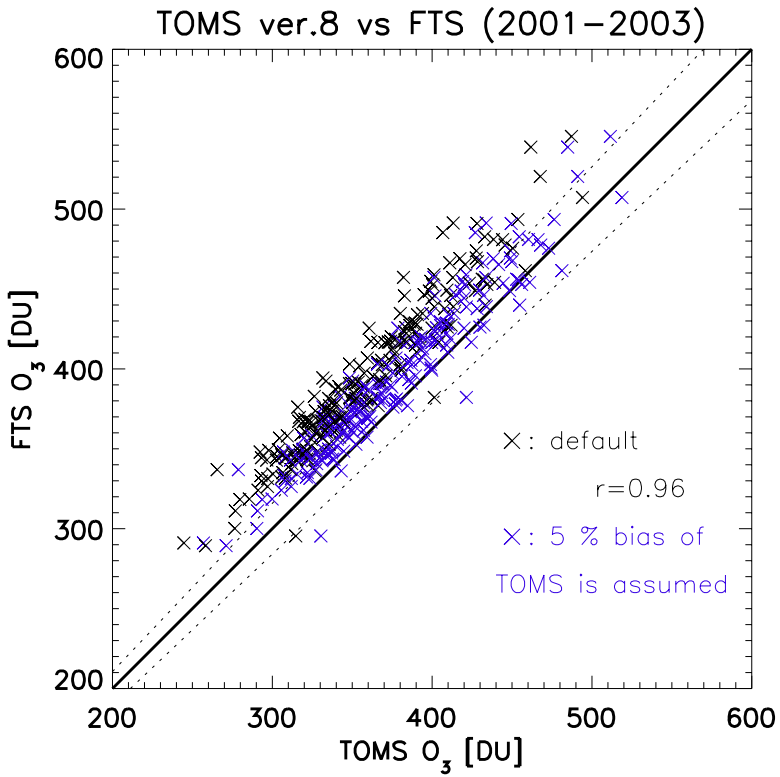

Fig. 6. Scatter plot of EP-TOMS data with FTS total ozone column. Black x's are the scatter plot of EP-TOMS and FTS ozone. The blue symbols are the same comparison of x but a 5% bias from the TOMS data is included. The solid line is the one-to-one line. The error range for the FTS total column ozone is also shown.

ACPD
6, 10299–10339, 2006

EGU

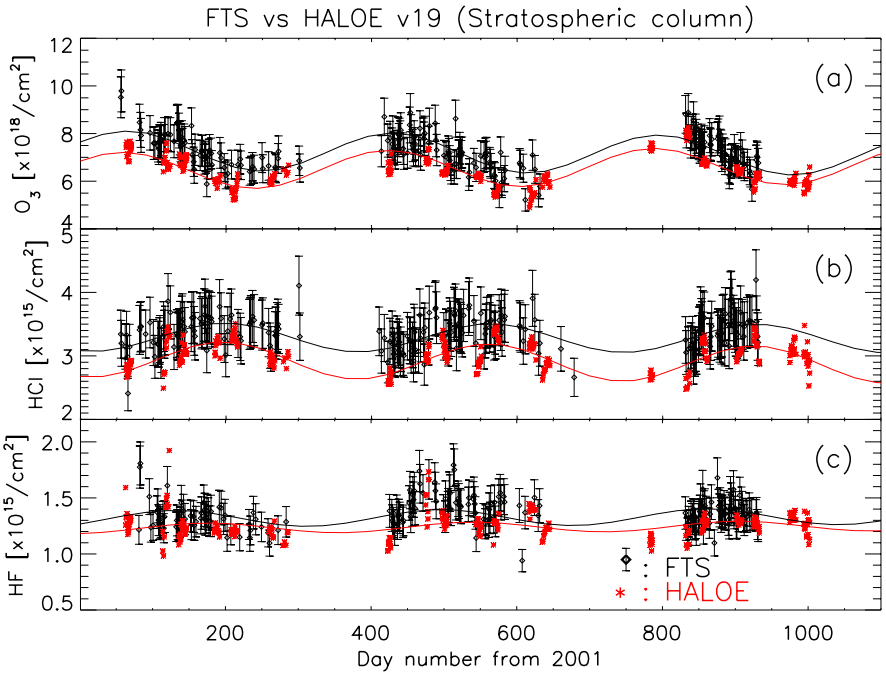

Fig. 7. (a) Comparison of stratospheric columns of FTS ozone and HALOE version 19 ozone from 2001 to 2003. The diamonds symbol with error bars indicates the FTS stratospheric ozone column. The FTS ozone error bars are taken from the 18–24 km partial column error (9.0%) estimated by the error analysis in Sect. 5.3. Red asterisk is the HALOE measurement. HALOE data within 10°latitude and 20°longitude of Poker Flat is plotted. Both the FTS and HALOE data are fitted using a function that includes terms for the seasonal cycle and annual trend. **(b)–(c)** are the same as (a) except for HCl, and HF. The error bars of the FTS derived HCl and HF are for the 20–40 km columns (11.3 and 10.6 %), respectively.

ACPD
6, 10299–10339, 2006

EGU

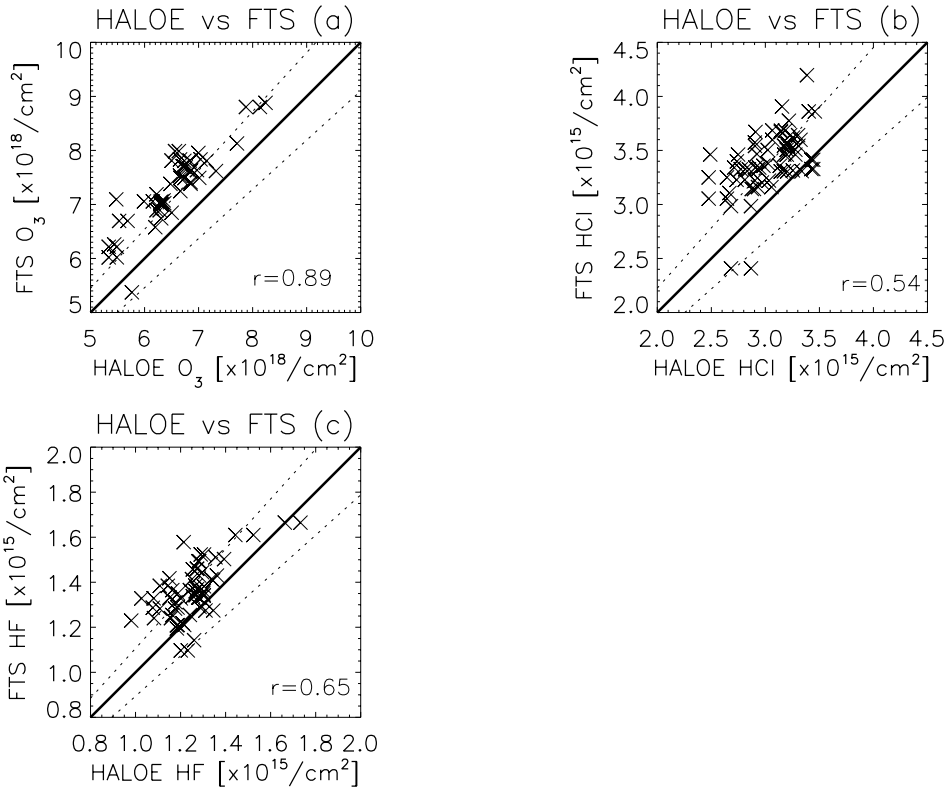

Fig. 8. (a) Scatter plot of HALOE and FTS ozone for the data displayed in Fig. 7a. Data for same-day measurements are plotted. **(b)–(c)** are the same as (a), except for HCl and HF.

ACPD
6, 10299–10339, 2006

EGU

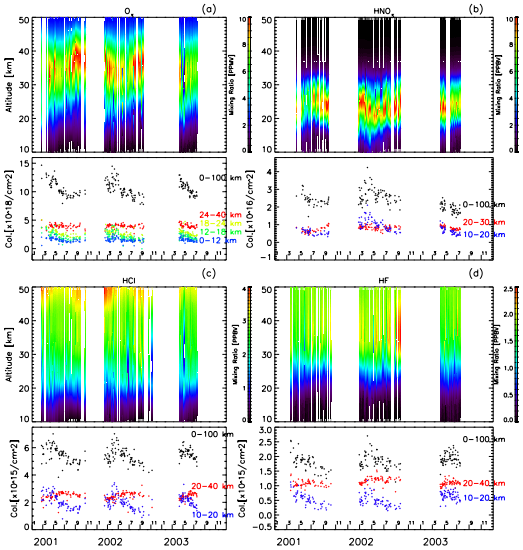

Fig. 9. (a) (upper panel) Time-height cross-section of ozone mixing ratio 10–50 km over Poker Flat from 2001 to 2003. The ozone mixing ratio scale is indicated with accompanying color bar. Data are plotted only for the period when observations and data retrieval were of sufficient quality and precision. When multiple observations were made on a single day, the observation nearest 15:00 (AKST) is selected for the plot which is the time at which the local sonde is flown and hence the source of the temperature data used in the FTS retrieval. (Lower panel) Black: Ozone total column for the same data as the upper panel. Blue: Ozone partial column for 0–12 km. Green: Ozone partial column for 12–18 km. Yellow: Ozone partial column for 18–24 km. Red: Ozone partial column for 24–40 km. **(b)** (upper panel) same as (a), except for HNO_3. (lower panel) Black: HNO_3 total column. Blue: HNO_3 partial column for 10–20 km. Red: HNO_3 partial column for 20–30 km. **(c)–(d)** (upper panels) same as (a), except for HCl or HF. (lower panels) Black: HCl and HF total column. Blue: HCl and HF partial column for 10–20 km. Red: HCl and HF partial column for 20–40 km.

ACPD
6, 10299–10339, 2006

EGU